J. Mech. Phys. Solids 153 (2021) 104483

Contents lists available at ScienceDirect

Journal of the Mechanics and Physics of Solids

journal homepage: www.elsevier.com/locate/jmps

# Flaw-sensitivity of a tough hydrogel under monotonic and cyclic loads

Yifan Zhou [a], Jian Hu [a], Pingping Zhao [b], Wenlei Zhang [a], Zhigang Suo [c,*], Tongqing Lu [a,*]

[a] State Key Lab for Strength and Vibration of Mechanical Structures, International Center for Applied Mechanics, Department of Engineering Mechanics, Xi'an Jiaotong University, Xi'an 710049, China
[b] Key Laboratory for Physical Electronics and Devices of the Ministry of Education & Shaanxi Key Lab of Information Photonic Technique, School of Electronic science and Engineering, Xi'an Jiaotong University, 710049, China
[c] John A. Paulson School of Engineering and Applied Sciences, Kavli Institute for Bionano Science and Technology, Harvard University, MA 02138, United States

ARTICLE INFO

*Keywords:*
Hydrogel
Fatigue
Endurance
Flaw-sensitivity length

ABSTRACT

Rupture of emerging tough hydrogels has received much attention in recent years. It is a fundamental question what length of initial flaws can significantly affect the rupture of a tough hydrogel. Here we study the rupture of a tough hydrogel, using samples with and without initial cuts, under monotonic and cyclic loads. We prepare six samples under the same conditions, either without initial cut, or with initial cuts of the same length, and load them monotonically to inspect the statistical variation of measured rupture stress, rupture stretch and work of rupture. We cycle the six samples in parallel to the same amplitude of stretch and record the number of cycles to rupture of each sample. The average number of cycles to rupture decreases with the amplitude of stretch; and an endurance stretch exists, below which the samples can sustain indefinite number of cycles without rupture. We find that when the initial cut is long, the endurance stretch decreases with the initial cut length. When the initial cut is short, the endurance stretch is insensitive to the initial cut length. We interpret this finding by a material-specific length, the endurance fractocohesive length. We compare the endurance fractocohesive lengths of the hydrogel and other materials, including elastomers, plastics, metals, and ceramics. It is hoped that similar experiments will be soon conducted for other hydrogels to guide their development.

## 1. Introduction

Since the 1960s, synthetic hydrogels have been developed in many fields of biointegration and bioinspiration (Fan and Gong, 2020). Examples include contact lenses (Caló and Khutoryanskiy, 2015; Wichterle, 1960), superabsorbent diapers (Masuda, 1994), tissue engineering (Lee et al., 2017; Liu et al., 2017; Zhang and Khademhosseini, 2017), drug delivery (Culver et al., 2017; Li and Mooney, 2016; Yuk et al., 2016), surgical adhesives (Li et al., 2017; Nam and Mooney, 2021; Yang et al., 2019b; Yuk et al., 2019b), bioelectronics (Liu et al., 2019; Yang and Suo, 2018; Yuk et al., 2019a), hydrophilic coatings (Parada et al., 2020; Yao et al., 2019), and soft robots (Yuk et al., 2017).

* Corresponding authors.
*E-mail addresses:* suo@seas.harvard.edu (Z. Suo), tongqinglu@mail.xjtu.edu.cn (T. Lu).

https://doi.org/10.1016/j.jmps.2021.104483
Received 7 February 2021; Received in revised form 4 May 2021; Accepted 4 May 2021
Available online 9 May 2021

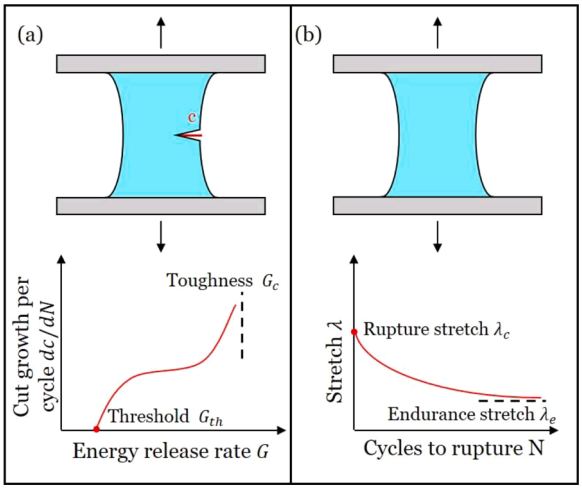


**Fig. 1.** Two kinds of fatigue tests. (a) Introduce an initial cut in a sample, cyclically stretch the sample, calculate the amplitude of the energy release rate, $G$, and record the cut growth per cycle, $dc/dN$. (b) Cyclically load a sample without initial cut to the amplitude of stretch, $\lambda$, and record the number of cycles to rupture, $N$.

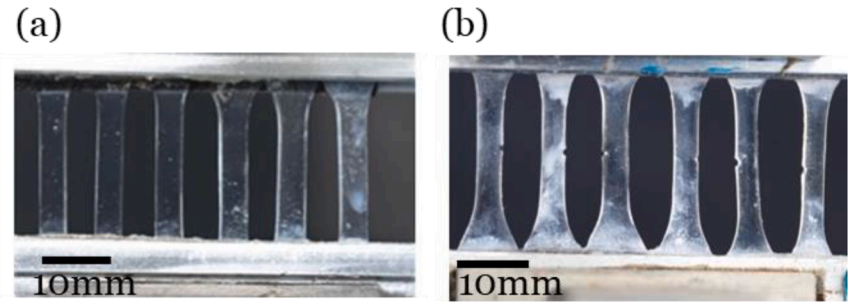


**Fig. 2.** The experimental setup for cyclic test. Six samples prepared under the same conditions are cycled in parallel, between two rigid grippers, to a given amplitude of stretch. (a) Six samples without initial cuts. (b) Six samples with initial cuts of the same length.

In many applications, hydrogels are required to sustain cyclic stretch. An artificial heart valve needs to open and shut ~30 million times a year (Butcher et al., 2011; Hasan et al., 2014). An artificial cartilage on the knee needs to sustain cyclic stress of amplitude ~2.5MPa (Yang et al., 2020). Hydrogel ionotronics, such as transparent loudspeakers, need to sustain high-frequency vibrations (Keplinger et al., 2013). The stretchable ionic touchpads need to survive cyclic deformation (Kim et al., 2016). Hydrogels are prone to a molecular disease: fatigue (Bai et al., 2019). Symptoms include change in properties (e.g., modulus and strength), as well as nucleation and growth of cracks. Fatigue of a material is commonly characterized by tests of many types, two of which will be used in this paper.

One type of fatigue test, initially developed to characterize elastomers (Thomas, 1958) and metals (Paris et al., 1961), is conducted as follows. Introduce a cut into a sample by scissors or a blade, cyclically stretch the sample, and record the cut growth per cycle as a function of the amplitude of energy release rate (Fig. 1a). The amplitude of energy release rate is between two limits: toughness $G_c$, at which the cut grows under monotonic stretch; and threshold $G_{th}$, at which the cut ceases to grow under cyclic stretch. According to this test, a material is said to be susceptible to fatigue if $G_{th} < G_c$. For example, natural rubber has toughness ~10,000 J/m$^2$ and threshold ~50 J/m$^2$ (Lake and Thomas, 1967). Since 2017, growth of cracks in hydrogels under cyclic stretch has been studied (Bai et al., 2018; Bai et al., 2017; Lin et al., 2019; Tang et al., 2017; Xiang et al., 2020; Zhang et al., 2018a; Zhang et al., 2018b; Zhang et al., 2018c; Zhou et al., 2020). All hydrogels tested so far, ranging from highly elastic hydrogels to plastically deformable hydrogels, are susceptible to fatigue crack growth.

A second type of fatigue test dates back at least to 1858 (Schütz, 1996). Such a test cyclically loads a material without initial cut to stretch of amplitude, $\lambda$, and records the number of cycles to rupture, $N$. The data are plotted as a point in the $\lambda - N$ plane (Fig. 1b). At a given amplitude of stretch $\lambda$, the number of cycles to rupture $N$ often scatters widely from sample to sample. The average number of cycles to rupture is a function of the amplitude of stretch. The amplitude of stretch is between two limits: the rupture stretch $\lambda_c$, at which the sample ruptures under monotonic stretch; and the endurance stretch $\lambda_e$, at which the sample survives indefinite number of cycles of stretch. According to this test, a material is said to be susceptible to fatigue if $\lambda_e < \lambda_c$. Similar data are also commonly plotted in the plane of amplitude of stress and the number of cycles to rupture. The data are commonly available for metals (Sharma et al., 2020), ceramics (Masuda et al., 1990), elastomers (Abraham et al., 2013), and composites (Ansari et al., 2018). Such data have become

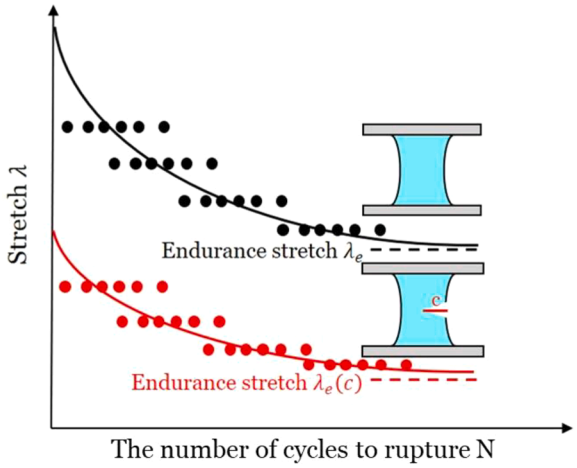


**Fig. 3.** Schematic of the plane of the amplitude of stretch, $\lambda$, and the number of cycles to rupture, $N$. For each run of the test, six samples are prepared either without initial cuts, or with initial cuts of the same length $c$. The six samples are cyclically stretched to the same amplitude, $\lambda$, and record the number of cycles to rupture, $N$. Plot the data of each sample as a point in the $\lambda - N$ plane. The endurance stretch is a function of the initial cut length, $\lambda_e(c)$.

available for a few hydrogels in recent years (Koshut et al., 2020a; Koshut et al., 2020b; Yang et al., 2020).

Here we study fatigue rupture of a tough hydrogel with and without initial cuts. To provide a basis for comparison, we first apply monotonic loads to samples with and without initial cuts to measure stress-stretch curves, rupture stretch, rupture stress, and work of rupture. We then apply cyclic loads to samples with and without initial cuts. To examine statistical variation, for each run of the test, we prepare six samples under the same conditions, either without initial cuts, or with initial cuts of the same length. We load the six samples in parallel, between two rigid grippers, to cyclic stretch of amplitude $\lambda$ (Fig. 2). For each sample, we plot the amplitude of stretch, $\lambda$, and the number of cycles to rupture, $N$, as a point in the $\lambda - N$ plane (Fig. 3). For sample without initial cut, the average number of cycles to rupture decreases with the amplitude of stretch, and an endurance stretch exists, $\lambda_e$, below which the samples can sustain indefinite number of cycles without rupture. For samples of a given initial cut length $c$, the average number of cycles to rupture also decreases with the amplitude of stretch. The endurance stretch of samples with initial cuts is a function of the initial cut length, $\lambda_e(c)$ (Fig. 3). When the initial cut is long, the endurance stretch decreases with the initial cut length. When the initial cut is short, the endurance stretch is insensitive to the initial cut length. We interpret this finding by a material-specific length, the endurance fractocohesive length. We compare the endurance fractocohesive lengths of the hydrogel and other materials, including elastomers, plastics, metals, and ceramics.

## 2. Sample preparation

We prepare a PAAm/PAMPS double-network hydrogel following the method of Gong et al. (2003). The substances are purchased from Aladdin: 1-acrylanmido-2-methylpropanesulfonic acid (AMPS, monomer), acrylamide (AAm, monomer), N,N' -methylenebis (acrylamide) (MBAA, crosslinker) and 2-oxoglutaric acid (OA, initiator). We formulate an aqueous solution of 1M AMPS with 4 mol-% MBAA and 0.1 mol-% OA relative to AMPS monomers. The solution is injected into a plastic mold covered with a pair of glass plates. The size of the glass plate is 15 mm×15mm. The mold is placed in a glovebox filled with nitrogen. The oxygen in the glovebox is less than 20ppm. In the glovebox, we place the mold under a 15 W and 365nm ultraviolet lamp for 8 h. A hard and brittle short-chain network of PAMPS hydrogel is formed. We immerse the prepared PAMPS hydrogel in an aqueous solution of 4M AAm, 0.01 mol-% MBAA and 0.01 mol-% OA relative to AAm for one day. After the immersion, the gel is sandwiched between two glass plates and placed in the same reaction cell as that in the first step. The prepared gel is immersed in deionized water for one day to swell and to remove the residual reactants. The hydrogel sample is prepared as a dumbbell-shaped sheet with the size of 17mm×4mm×1.5mm. We introduce the initial cuts of length $65 \pm 10\mu m$ by using a femtosecond laser (Libra-USP-HE, Coherent Inc., U.S.). To introduce larger cuts of length 0.4mm, 0.5mm and 1mm, we fabricate three custom-made metallic cutters. In the middle of the cutter, we make a line of metal as the razor blade with the length 0.4mm, 0.5mm and 1mm. The hydrogel samples are prepared using the three cutters, and the measured initial cut length is $400.5 \pm 6.9\mu m$, $504.8 \pm 12.1\mu m$ and $997.0 \pm 36.3\mu m$. The mean and variance are calculated from 6 samples of each cut length.

## 3. Rupture under monotonic stretch

### 3.1. Statistics of samples under monotonic stretch

We monotonically stretch each sample with or without an initial cut. The stretch rate is 100 mm/min for all the tested samples. The

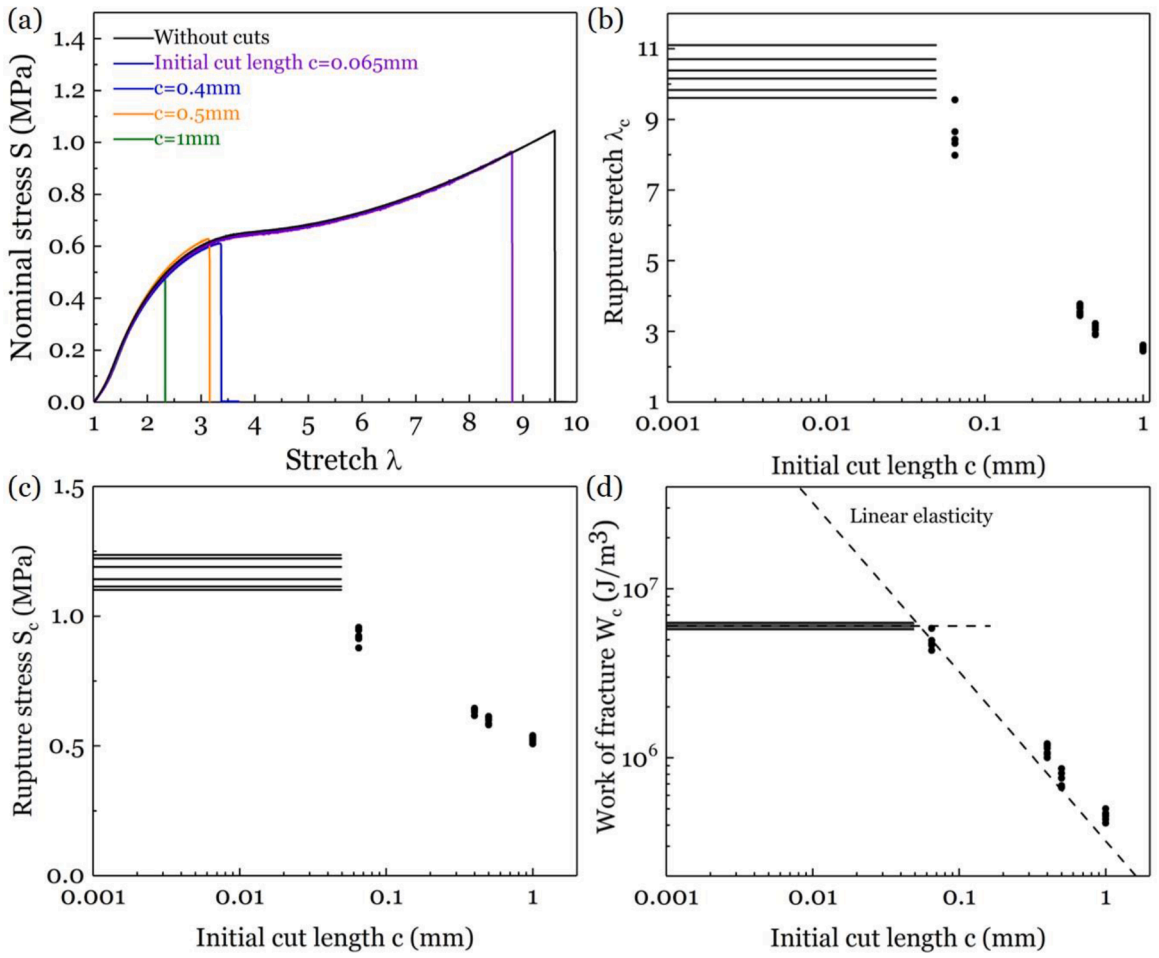


**Fig. 4.** Samples without initial cuts and with initial cuts of various lengths under monotonic load. (a) Stress-stretch curves. (b) The plane of rupture stretch $\lambda_c$ and the initial cut length $c$. In the $\lambda_c$-$c$ plane, each data point corresponds to a sample with an initial cut, and each horizontal segment corresponds to a sample without initial cut. (c) The plane of rupture stress $S_c$ and the initial cut length $c$. (d) The plane of the work of rupture $W_c$ and the initial cut length $c$. Also included is the prediction of linear elastic fracture mechanics. The corresponding horizontal line intersects with the prediction at a length $\sim 50\mu m$.

stretch $\lambda$ is defined by the deformed length of the sample divided by its undeformed length. The nominal stress $S$ is defined by the force divided by the cross-sectional area of the undeformed and uncut sample. For samples without initial cuts, these definitions are commonly used. For samples with initial cuts, these definitions are adopted here as a convention. With this convention, the area under a stress-stretch curve is the work done by the tensile tester on the sample divided by the volume of the sample. This statement is correct for all samples, with or without initial cuts.

To inspect statistical variation from sample to sample, we test six samples without any initial cut. For visual clarity, we only plot a representative stress-stretch curve of one of the six samples (Fig. 4a). This sample ruptures at stretch $\lambda_c = 9.59$ and stress $S_c = 1.04$MPa. The area under the stress-stretch curve gives the work of rupture, $W_c = 5.87 \times 10^6 \mathrm{J/m^3}$. For samples with initial cuts of each length, we also test six samples, and plot a representative stress-stretch curve. For example, the sample with the initial cut length $c = 0.4$mm ruptures at stretch $\lambda_c = 3.38$, stress $S_c = 0.61$MPa, and work of rupture $W_c = 9.2 \times 10^5 \mathrm{J/m^3}$. We will characterize statistics of all these samples later.

Each sample with an initial cut gives a point in the plane of rupture stretch $\lambda_c$ and the initial cut length $c$ (Fig. 4b). Samples without initial cuts may contain flaws of unknown lengths. A flaw on the order of $50\mu m$ would be easily visible in a microscope. Since we do not observe such flaws, we take lengths of the flaws to be below $50\mu m$, and plot each sample without initial cut by a horizontal segment terminated at $50\mu m$. The points and segments are also marked in the plane of rupture stress $S_c$ and initial cut length $c$ (Fig. 4c), as well as in the plane of the work of rupture $W_c$ and initial cut length $c$ (Fig. 4d).

We measure the scatter of each property by a dimensionless number, the coefficient of variation ($CV$), defined by the standard deviation divided by the mean (Fig. 5). In addition to rupture stretch $\lambda_c$, rupture stress $S_c$, and work of rupture $W_c$, we also include stiffness $M$, defined by the slope of the stress-stretch curve at small stretch. The scatters are small ($CV < 0.1$) and comparable for all the four properties, for samples with and without initial cuts.

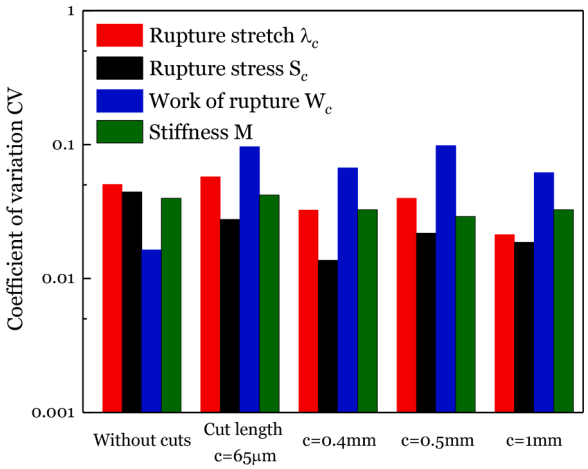


**Fig. 5.** Coefficients of variation of rupture stretch, rupture stress, work of rupture and stiffness for samples, with or without initial cuts, ruptured by monotonic loads.

### 3.2. Toughness measured using samples with initial cuts

A sample with an initial cut is commonly analyzed using energy release rate $G$ (Rivlin and Thomas, 1953). When the cut is much smaller than the sample, a dimensional consideration dictates that the energy release rate, $G$, should take the form (Rivlin and Thomas, 1953):

$$G = kWc, \tag{1}$$

where $c$ is the length of the cut, $W$ is the density of the elastic energy remote from the cut, and $k$ is a dimensionless number calculated by solving the boundary value problem of elasticity. Thus, $k$ depends on the applied stretch $\lambda$, and may also depend on the dimensionless elastic constants. For a material of linear elasticity, the stress is linear in stretch, $S = E(\lambda - 1)$, where $E$ is Young's modulus. The density of elastic energy is quadratic in stress, $W = S^2/2E$. The dimensionless number $k$ is $2\pi$ for a center-cracked sample and is $2\pi(1.122)^2$ for an edge-cracked sample (Tada et al., 2000). For a Gent material, the density of elastic energy is a nonlinear function of stretch and stress, and $k$ is a complicated function $k(\lambda, J_{\lim})$, where $J_{\lim}$ is the dimensionless parameter in the Gent model (Chen et al., 2017; Greensmith, 1964). For the material studied in this paper, the PAAm-PAMPS double network hydrogel, the Gent model does not fit the stress-stretch curve well so that the specific form of $k$ is even more complicated. In the following, we simply use the prediction of linear elasticity to qualitatively compare with the experiment.

When the sample ruptures, Eq. (1) relates the rupture stretch $\lambda_c$ to the critical energy release rate, $G_c$. When the length of the cut, $c$, is large compared to a material-specific length, to be discussed below, $G_c$ is a material-specific constant, independent of the length of the cut and the shape of the sample. This material-specific constant, $G_c$, is called the toughness. The toughness of this hydrogel has been measured before, $G_c = 2550J/m^2$ (Zhou et al., 2020). With the simplification of linear elasticity, along with the measured toughness, $G_c = 2550J/m^2$, the equation $G = kWc$ is a straight line in the $W_c - c$ plane (Fig. 4d). This straight line roughly predicts our experimental data of rupture of samples with initial cuts. The comparison is surprisingly good since we do not expect a quantitative comparison between the prediction of linear elasticity with the experimental data. Rupture of a sample with an initial cut is caused by the growth of the cut. According to Eq. (1), the rupture properties are predicted by the toughness $G_c$ and the elastic energy density function $W$. Our data indicate that rupture properties scatter narrowly (Figs. 4, 5). Consequently, the toughness $G_c$ must also scatter narrowly. This finding is consistent with the common practice that regards $G_c$ as a material constant.

### 3.3. Work of rupture measured using samples without initial cuts

Let us next focus on samples without initial cuts. The scatters of the rupture properties, $\lambda_c$, $S_c$, and $W_c$, are comparable to the scatter of small-stretch stiffness, $M$ (Fig. 5). Our finding here for the tough hydrogel is comparable to that for a polyacrylamide hydrogel (Yang et al., 2019a). This finding for the hydrogels, however, is in stark contrast with the experience with brittle solids, such as silica. For silica, the scatter of rupture stress is enormous (Proctor et al., 1967), but the scatter of stiffness is small (Davidge and Evans, 1970). The following story for silica has been told many times since the work of Griffith (1921). Rupture in silica is caused by stress concentration at the tip of a cut-like flaw. Rupture stress scatters widely because rupture stress is set by the flaw of extreme size. The stiffness of silica comes from small distortion of the election clouds of covalent bonds under stretch. Stiffness scatters narrowly because the stiffness is set by the average behavior of all covalent bonds. For silica, stiffness is a material constant, but rupture stress is not. For the hydrogel, however, our data show that the rupture properties scatter as narrowly as stiffness. For samples without initial cuts, all four quantities, $\lambda_c$, $S_c$, $W_c$, and $M$, are material constants.

### 3.4. Fractocohesive length

For samples without initial cuts (c = 0) and with initial cuts ($c \neq 0$), the work of rupture is a function, $W_c(c)$. In the $W_c$-$c$ plane, our data scatter narrowly around the two straight lines (Fig. 4d). The horizontal line defines one material constant, $W_c(0)$, the work of rupture measured using samples without initial cuts. The inclined line defines another material constant, $G_c$, the toughness measured using samples with long initial cuts. When the initial cut is short, the condition for rupture is insensitive to the cut. That is, the rupture properties $\lambda_c$, $S_c$ and $W_c$ of a sample with a short initial cut are the same as those of a sample without initial cut (Fig. 4). When the initial cut in a sample is long, the rupture properties are smaller than the values of a sample without initial cut. The transition takes place at a cut length, which is called the flaw-sensitivity length, $c_c$. This length is also called the "inherent flaw size" (Berry, 1961). The flaw-sensitivity length can be determined by the two material constants, $G_c$ and $W_c(0)$ as

$$c_c = \frac{1}{k}\frac{G_c}{W_c(0)}. \tag{2}$$

The flaw-sensitivity length $c_c$ scales with the ratio $G_c/W_c(0)$, which is discussed below. For the hydrogel tested in this paper, the work of rupture measured using samples without initial cuts is $W_c(0) = 5.9 \times 10^6 \mathrm{J/m^3}$, and the toughness measured using samples with long initial cuts is $G_c = 2550 J/m^2$. With the simplification of linear elasticity, $k = 2\pi(1.122)^2$, the flaw-sensitivity length of the hydrogel is estimated to be $c_c = 0.05mm$.

The rupture of a material is now characterized with four material constants: rupture stretch $\lambda_c(0)$, the rupture stress $S_c(0)$, and the work of rupture $W_c(0)$ measured using a sample without initial cut, as well as the toughness $G_c$ measured using a sample with a long initial cut. The ratio of two of these material constants, $G_c/W_c(0)$, defines yet another material constant, of dimension of length, called the fractocohesive length (Chen et al., 2017; Yang et al., 2019a). The fractocohesive length of this hydrogel is $G_c/W_c(0) = 0.432$ mm.

The ratio $G_c/W_c(0)$ has received little attention, but dates back to the early days of fracture mechanics (Thomas, 1955). Thomas introduced incision of various tip diameters, $d$, in sheets of natural rubber, and measured the critical energy release rate, $G_c$. He also measured the work of rupture $W_c(0)$ of the natural rubber using a sample without initial cut. His data showed the approximate relation $G_c \approx W_c(0)d$. In his experiment, $W_c(0)$ is a material constant, but neither $d$ nor $G_c$ is. Towards the end of his paper, Thomas noted the following. In conventional measurement of toughness, where the incision (i.e., the cut) is made by a sharp blade, the measured $G_c$ is a material constant, so that the ratio $G_c/W_c(0)$ is also a material constant. He further noted that this material constant $G_c/W_c(0)$ is about the same size as irregularities developed on the crack surface.

The relation $G_c \approx W_c(0)d$ is linked to energy dissipation accompanying crack growth (Greensmith, 1960). As a cut grows in a sample, energy dissipates in layers of the material above and below the cut plane. The energy dissipated per unit volume is taken to be the same as the work of rupture measured using a sample without initial cut, $W_c(0)$. In effect, Greensmith identified the length $d$ as the size of the fracture process zone. Let $d$ be the total thickness of the dissipation layers, and $B$ be the thickness of the sample. When the cut grows by $\Delta c$, the energy dissipated is $W_c(0)dB\Delta c$. Consequently, the energy dissipated per unit area of the cut growth is $W_c(0)d$, which is $G_c$.

The fractocohesive length $G_c/W_c(0)$ is determined by two independent measurements: the work of fracture, $W_c(0)$, measured by the rupture of a sample without initial cut, and the toughness, $G_c$, measured by the rupture of a sample with a long initial cut. The fractocohesive length is a material constant, so long as $W_c(0)$ and $G_c$ are material constants. Here we call a quantity a material constant if the quantity scatters narrowly, which can be ascertained by running each test multiple times. For a given material, determining its fractocohesive length experimentally may not be always easy. For a brittle material, such as silica, the fractocohesive length is ~ 1 nm, which is too small for the resolution in which flaws are commonly observed. For a ductile material, such as a soft metal, the fractocohesive length may go beyond 10 cm, which requires samples too large to be practical.

In the above, we have recalled that the fractocohesive length $G_c/W_c(0)$ scales other lengths, including the flaw-sensitivity length (Chen et al., 2017), the irregularities on the crack surface (Thomas, 1955), and fracture process zone size (Greensmith, 1960). Conceivably, the fractocohesive length $G_c/W_c(0)$ scales other lengths of interest. For example, two rubbery polymers can adhere when their networks are in topological entanglement with glassy polymer particles, which are called molecular staples (Chen et al., 2019). The stress concentration around the glassy particles do not lower adhesion if they are small compared to a material length, which should scale with the fractocohesive length.

## 4. Rupture under cyclic stretch

### 4.1. Statistics of samples under cyclic stretch

We cyclically stretch each sample with or without initial cut. In each run of a test, six samples are cyclically stretched in parallel between two rigid grippers (Fig. 2). To achieve strong bonding during the prolonged cyclic tests, we dip the ends of each sample for 3 s in an aqueous solution $Ca(HCO_3)_2$ of ~pH 8. Then the ends of the samples are attached to aluminum alloy plates using cyanoacrylate glue. We also use clips to bind the aluminum alloy plates to further secure the samples. The aluminum alloy plates are fixed to rigid grippers of the tensile tester with a 500N load cell (SHIMADZU AGS-X). We apply a triangular cyclic stretch to the samples from the minimum stretch 1 to a given amplitude of stretch $\lambda$. The loading rate is 10 mm/s.

We run the test of six samples of PAAm-PAMPS hydrogel without initial cuts. The tensile tester records the maximum force applied to the grippers cycle by cycle. The hydrogel has two interpenetrating networks: the PAAm network has long polymer chains, and the

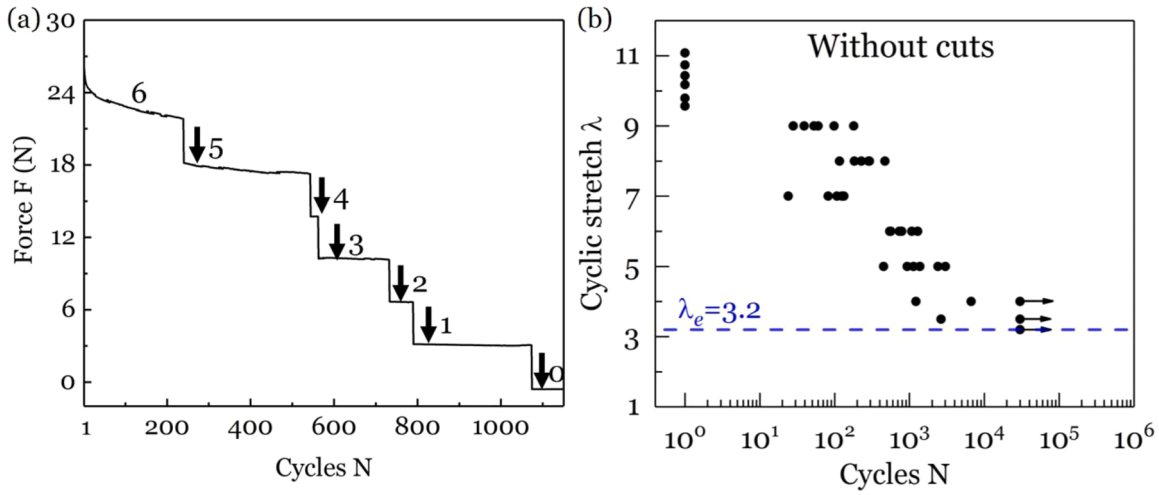


**Fig. 6.** Fatigue test of samples without initial cuts. In each run of the test, six samples are cyclically loaded in parallel with a stretch of amplitude, $\lambda$. (a) During the test, the force applied to the grippers is recorded. When one of the six samples ruptures, the force drops sharply, as indicated by a vertical arrow, and the number of cycles is recorded. For this plot, the amplitude of stretch is $\lambda = 6$. (b) In the $\lambda - N$ plane, a data point represents a ruptured sample, and horizontal arrow represents a survived sample. Each run of the test terminates at 30,000 cycles. Also included in the $\lambda - N$ plane are six samples ruptured by monotonic stretch.

PAMPS network has short chains. In the first cycle, the PAMPS network damages extensively, leading to a sharp drop in force. In the subsequent cycles, the PAMPS network damages further, leading to gradual drop in force. When one of the six samples ruptures, the force drops sharply. Consequently, the force-cycle curve gives the number of cycles at which each sample ruptures. For example, at the amplitude of stretch $\lambda = 6$, the force-cycle curve identifies the numbers of cycles to rupture of the six samples: 240, 544, 563, 733, 790, and 1074 (Fig. 6a). These data correspond to six points in the plane of two axes: the amplitude of stretch and the number of cycles to rupture, $\lambda - N$ (Fig. 6b).

If a run of the test still has one or more survival samples at 30,000 cycles, we terminate the test, and draw a horizontal arrow in the $\lambda - N$ plane. The number "30,000" is picked so that a run of test is finished in a reasonable amount of time. Each cycle takes about 10 s, and a run of test of 30,000 cycles takes about a few days. For a run of test at $\lambda = 4$, four samples survive 30,000 cycles, and we plot an arrow from the point $\lambda = 4$ and $N = 30{,}000$. For a run of test at $\lambda = 3.2$, all six samples survive, and we plot a horizontal arrow from the point $\lambda = 3.2$ and $N = 30{,}000$. The endurance stretch $\lambda_e$ is taken to be the largest amplitude of stretch tested, in which all six samples survive 30,000 cycles. The endurance stretch of the hydrogel without initial cuts is $\lambda_e = 3.2$. Also included in the $\lambda - N$ plane are six samples ruptured by monotonic stretch, represented by points at the rupture stretches $\lambda_c$ and $N = 1$.

Following the above procedure, we run tests using samples with initial cuts. Each run of the test cyclically loads six samples of initial cuts of the same length $c$, to amplitude of stretch $\lambda$, up to 30,000 cycles. Fig. 7(a) shows a representative curve of the recorded force versus the number of cycles. For the samples with initial cuts, the crack grows steadily and a sharp load drop is observed when one of the six samples ruptures. We run tests for samples with initial cuts of the four lengths: 65$\mu m$, 0.4mm, 0.5mm, 1 mm (Fig. 7b–7e). The endurance stretch is a function of the initial cut length, $\lambda_e(c)$. Our tests determine the endurance stretches 2.8, 2.1, 1.9, and 1.5 for the samples of four initial cut lengths.

For samples without initial cuts, endurance stretch $\lambda_e = 3.2$ is plotted as a horizontal segment up to 50$\mu m$ in the $\lambda_e$-$c$ plane (Fig. 8a). In the 30,000$^{\text{th}}$ cycle, we plot the average stress of the six samples as a function of stretch (Fig. 8b). The stress-stretch curve exhibits a large residual stretch due to damage (Zhang et al., 2018d; Zhou et al., 2020). At the endurance stretch, the corresponding average stress is called the endurance stress $S_e$, which is plotted as a horizontal segment in the $S_e$-$c$ plane (Fig. 8c). The area under the stress-stretch curve defines the endurance work $W_e$, which is plotted as a horizontal segment in the $W_e$-$c$ plane (Fig. 8d).

For samples with initial cuts of an initial length $c$, the endurance stretch $\lambda_e(c)$ is plotted as a point in the $\lambda_e$-$c$ plane (Fig. 8a). In the 30,000th cycle, we plot the average stress of the six samples as a function of stretch (Fig. 8b). We plot the endurance stress as a point in the $S_e$-$c$ plane (Fig. 8c), and the endurance work $W_e$ as a point in the $W_e$-$c$ plane (Fig. 8d).

The number of cycles to rupture scatters among the six samples in each run of the test (Fig. 9). Among the six samples in a run of the test, the numbers of cycles to rupture easily differ by an order of magnitude. The large scatter is commonly observed in fatigue tests for almost all materials. For each run of the test in which all six samples rupture before 30,000 cycles, define the coefficient of variation ($CV$) of the number of cycles to rupture as the standard deviation divided by the mean. The scatter among the samples in each run of the test is large ($CV \sim 1$). Furthermore, the scatter among the samples without initial cuts is comparable to the scatter among the samples with initial cuts.

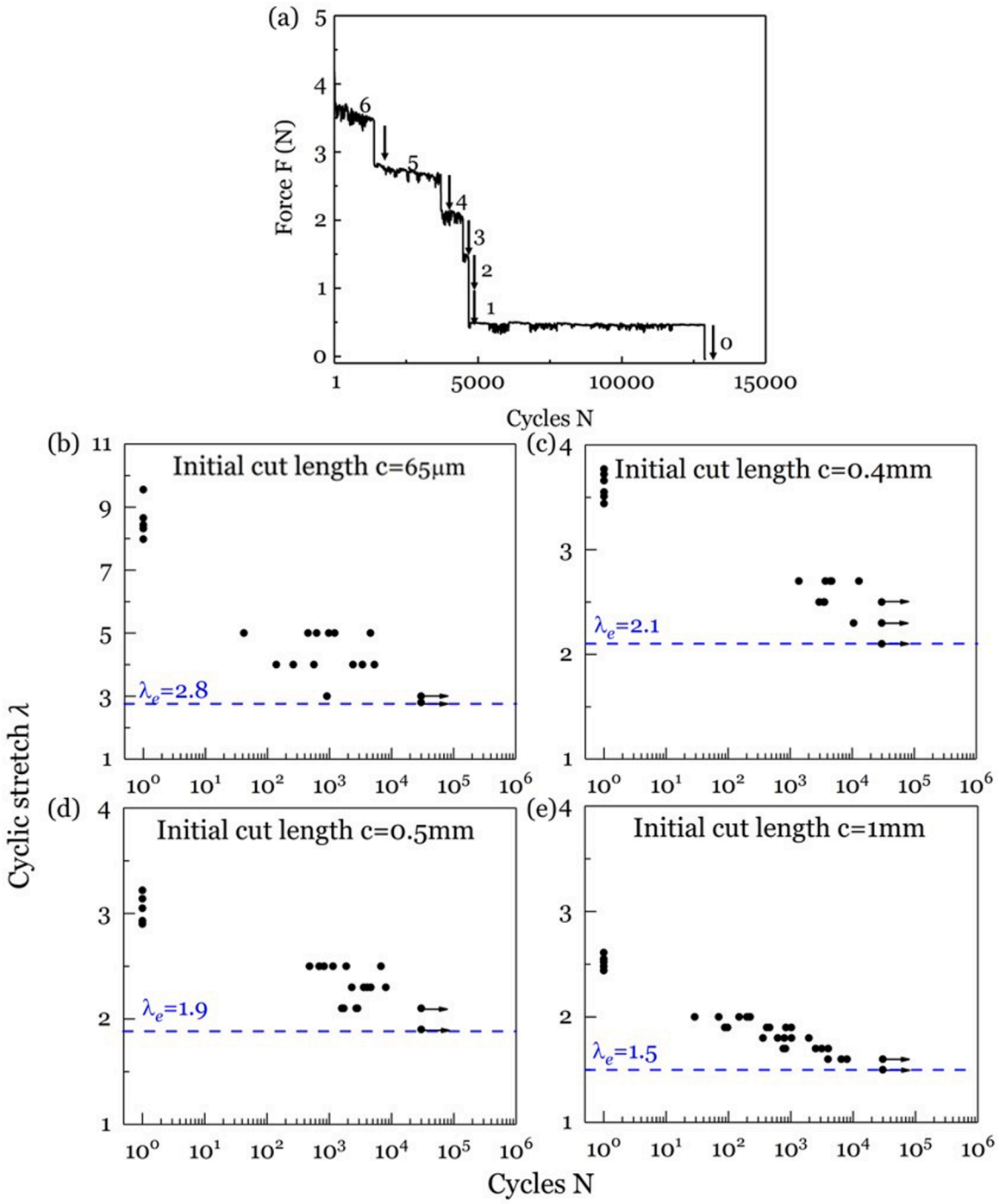


**Fig. 7.** Fatigue test of samples with initial cuts. In each run of the test, six samples with initial cuts of the same length, $c$, are cyclically loaded in parallel to a stretch of amplitude, $\lambda$. (a) A representative curve of the recorded force versus the number of cycles. When one of the six samples ruptures, the force drops sharply. For this plot, the initial cut of the samples is 0.4mm and the amplitude of stretch is $\lambda = 2.7$. The $\lambda - N$ curves of samples with initial cuts of different lengths (b) 65$\mu m$. (c) 0.4mm. (d) 0.5mm. (e) 1 mm. Each run of the test terminates at 30,000 cycles.

### *4.2. Threshold measured using samples with initial cut*

For samples with cuts of initial length $c$, Eq. (1) relates stretch to energy release rate. When the endurance limit is reached, Eq. (1) relates the endurance work $W_e$ to the critical energy release rate, $G_{th}$. When the length of the cut, $c$, is large compared to a material-specific length, to be discussed below, $G_{th}$ is also a material-specific constant, independent of the length of the cut and the shape of the

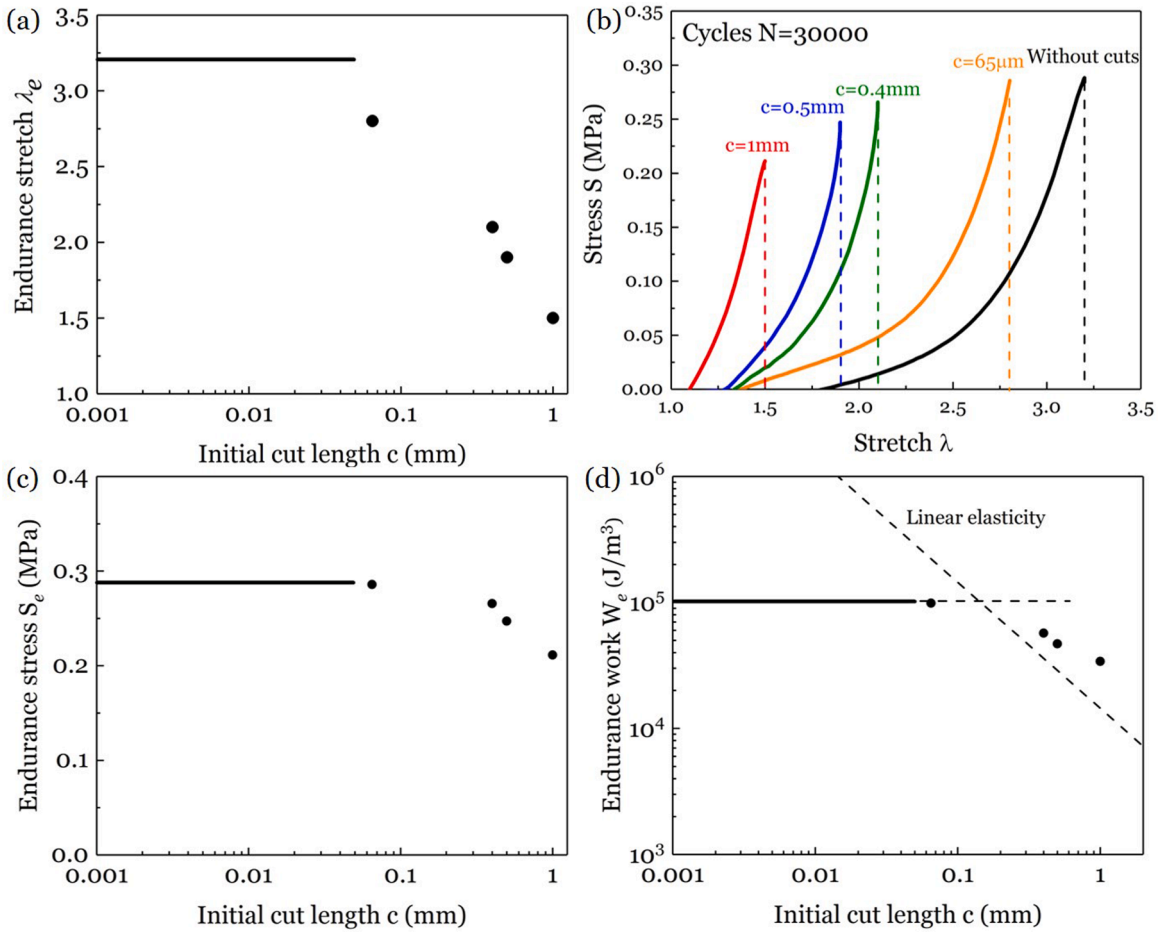


**Fig. 8.** Endurance limits of samples without initial cuts and with initial cuts of various lengths. (a) The $\lambda_e$-$c$ plane. (b) At each value of $\lambda_e(c)$, the average stress-stretch curve of the six samples is measured in the 30,000th cycle. (c) The $S_e$-$c$ plane. (d) The $W_e$-$c$ plane.

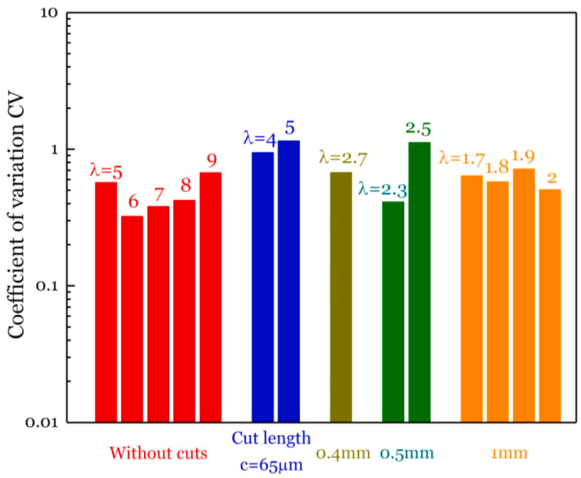


**Fig. 9.** The number of cycles to rupture scatters widely among the six samples in each run of the test. The scatter among the samples without initial cut is comparable to the scatter among the samples with initial cuts. Each bar represents a run of the test in which all six samples rupture before 30,000 cycles.

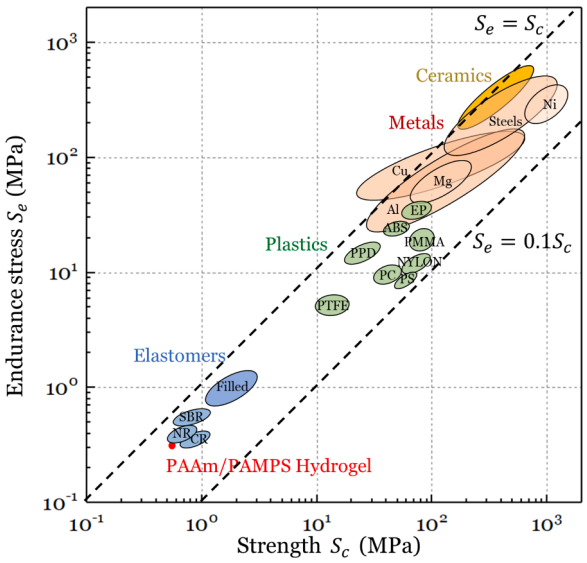


**Fig. 10.** The plane of the endurance stress measured under cyclic load and strength measured under monotonic load. Metals include aluminum alloys (Al), magnesium alloy (Mg), cooper alloys (Cu), nickel alloys (Ni), iron alloys (Steels), Plastics include acrylonitrile butadiene styrene (ABS), epoxy resin (EP), polycarbonate (PC), polystyrene (PS), polymethyl methacrylate (PMMA), polyphenylene oxide (PPO), poly tetra fluoroethylene (PTFE), polycarbonate (Nylons). Elastomers include natural rubber (NR), polymerized styrene butadiene rubber (SBR), chloroprene rubber (CR), filled rubber (Filled).

sample. This material-specific constant, $G_{th}$, is called the threshold. The threshold of this hydrogel has been measured before, $G_{th} = 114.2J/m^2$ (Zhou et al., 2020). For a material of linear elasticity, along with the measured threshold, $G_{th} = 114.2J/m^2$, the equation $G_{th} = kW_e c$ is a straight line in the $W_e - c$ plane (Fig. 8d). This straight line roughly predicts our experimental data of endurance work of samples with initial cuts.

### 4.3. Endurance fractocohesive length

In the $W_e$-$c$ plane, the horizontal line corresponds to the endurance work $W_e(0)$ measured using samples without initial cuts. The inclined line is approximately predicted by the LEFM using the threshed $G_{th}$ measured using samples with long initial cuts. When the initial cut is short, the condition for fatigue rupture is insensitive to the cut. That is, the endurance properties, $\lambda_e$, $S_e$, and $W_e$, of a sample with a short cut are the same as those of a sample without initial cut (Fig. 8). When the initial cut in a sample is long, the endurance properties of the sample are smaller than the values of a sample without initial cut. The transition takes place at a cut length, which is called the endurance flaw-sensitivity length, $c_e$. The endurance flaw-sensitivity length can be determined by the two material constants, $G_{th}$ and $W_e(0)$ as

$$c_e = \frac{1}{k}\frac{G_{th}}{W_e(0)}. \tag{3}$$

The endurance flaw-sensitivity length $c_e$ scales with the ratio $G_{th}/W_e(0)$. For the hydrogel tested in this paper, $W_e(0) = 1.02 \times 10^5 \mathrm{J/m^3}$ and $G_{th} = 114.2J/m^2$. We use linear elasticity to estimate $c_e = 0.116\frac{G_{th}}{W_e(0)}$ to be 0.13mm (Fig. 8d).

The endurance of a material is now characterized with four material constants: endurance stretch $\lambda_e(0)$, endurance stress $S_e(0)$, and endurance work $W_e(0)$ measured using samples without initial cuts, as well as the threshold $G_{th}$ measured using samples with long initial cuts. The ratio of two of these material constants, $G_{th}/W_e(0)$, defines yet another material constant, of dimension of length, called the endurance fractocohesive length. The endurance fractocohesive length of the hydrogel is $G_{th}/W_e(0) = 1.1$ mm.

## 5. Space of properties

For a material without initial cut, the ability to withstand monotonic load is characterized by strength $S_c$ and the elastic limit strain $\varepsilon_c$. For an elastic material like a ceramic and elastomer, the strength $S_c$ is the rupture strength, and the elastic limit strain $\varepsilon_c$ is the rupture strain. For an inelastic material like a metal and plastic, the strength $S_c$ is taken as the yield strength, and the elastic limit strain $\varepsilon_c$ is the strain corresponding to the stress $S_c$. The ability to resist cyclic load is characterized by endurance stress $S_e$ and the corresponding endurance strain $\varepsilon_e$. The determination of $S_e$ and $\varepsilon_e$ is similar to that under monotonic load. The strain is related to stretch as $\varepsilon = \lambda - 1$.

The hydrogel used in this paper is a typically inelastic material: the stress-stretch curve has a clear plateau (Fig. 4a), accompanied with the observation of necking in the tensile experiment, and a large hysteresis (Gong, 2010). The yield strength is $S_c = 0.5$ MPa, and

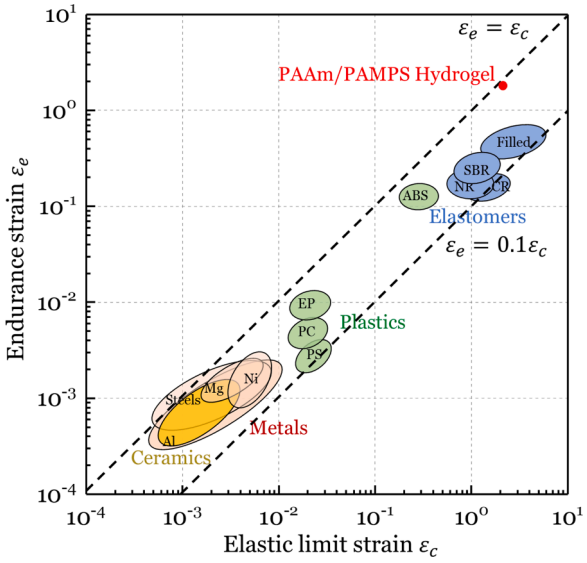


**Fig. 11.** The plane of the endurance stretch measured under cyclic load and elastic limit strain measured under monotonic load.

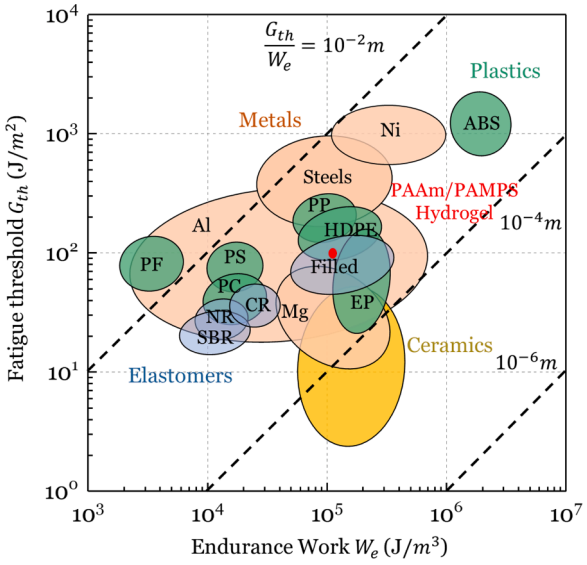


**Fig. 12.** The plane of the endurance work measured under cyclic load and fatigue threshold measured under monotonic load. The inclined dashed lines indicate the endurance fractocohesive length, $G_{th}/W_e(0)$.

the elastic limit is $\varepsilon_c = 2$. The endurance stress is $S_e = 0.28$ MPa, and the endurance strain is $\varepsilon_e = 2.2$.

Fig. 10 collects the data of elastomers, plastics, ceramics, metals in the $S_e - S_c$ plane (Fleck et al., 1994). The ratio $S_e/S_c$ is often used to evaluate the fatigue resistant property for materials without initial cut. The ratio is 1 for ceramics, about 0.5 for metals and elastomers, and about 0.3 for polymers. For the PAAm/PAMPS hydrogel, the ratio $S_e/S_c = 0.56$.

Fig. 11 plots the data of elastomers, plastics, ceramics, metals in the $(\varepsilon_e, \varepsilon_c)$ plane. For ceramics, the stress-strain relation is linear up to rupture, and the elastic limit strain $\varepsilon_c$ is determined by the rupture stress $S_c$ by $\varepsilon_c = S_c/E$, where $E$ is Young's modulus. For metals and plastics, the stress-strain relation is linear before yielding, and the elastic limit strain $\varepsilon_c$ is determined by the yielding stress $S_c$ by $\varepsilon_c = S_c/E$. The endurance strain $\varepsilon_e$ is determined similarly. For elastomer, the elastic limit strain and endurance strain are read from the stress-strain curve corresponding to the rupture stress and endurance stress from literature (Dizon et al., 1974; Gent and Tobias, 1982; Greensmith, 1956; Greensmith et al., 1960; Gregg and Macey, 1973; Lake, 1966; Lake, 1972; Neogi et al., 1990; Rivlin and Thomas, 1953; Royo, 1992). The endurance strain is about 0.1-1 for elastomers, $10^{-2}$ for plastics, $10^{-3}$ for metals and ceramics. The single point for PAAm/PAMPS hydrogel has the elastic limit strain of 2 and the endurance strain of 2.2.

For materials under monotonic load, if the initial cut length is large, the ability to resist crack growth is characterized by toughness

$G_c$. If the initial cut length is small and the material is insensitive to the cut, the ability to resist rupture is characterized by the work of rupture $W_c(0)$. Data of various materials have been plotted before in the plane of $(G_c, W_c(0))$ (Chen et al., 2017). These two material properties give the fractocohesive length $G_c/W_c(0)$.

For materials under cyclic load, if the initial cut length is large, the ability to resist crack growth is characterized by fatigue threshold $G_{th}$. If the initial crack length is small and the material is insensitive to the crack, the ability to resist fatigue rupture is characterized by the endurance work $W_e(0)$. Fig. 12 collects the available data of elastomers, plastics, ceramics, metals (Fleck et al., 1994) in the plane of threshold and endurance work $(G_{th}, W_e(0))$. Fatigue threshold is often represented by the stress intensity factor $K_{th}$ in the literature. For metals, ceramics and plastics, we use an approximation of linear elasticity to transfer $K_{th}$ to $G_{th}$ by $G_{th} = {K_{th}}^2/E$. We also transfer endurance stress $S_e$ to endurance work $W_e(0)$ by $W_e(0) = {S_e}^2/2E$. For elastomers, we directly report the measured $G_{th}$ and $W_e(0)$ in literature (Bhowmick et al., 1983; Dizon et al., 1974; Gent et al., 1964; Gent and Tobias, 1982; Lake, 1972; Lake and Thomas, 1967; Lindley, 1964; Royo, 1992). The two material properties under cyclic loads $G_{th}$ and $W_e(0)$ give the endurance fractocohesive length $G_{th}/W_e(0)$, which is indicated by the inclined dashed lines (Fig. 12). For example, ceramics have the endurance fractocohesive length on the order of $10^{-4}m$, steel and the PAAm/PAMPS hydrogel have the endurance fractocohesive length on the order of $10^{-3}m$.

## 6. Concluding remarks

We study rupture of a hydrogel, using samples with and without initial cuts, under monotonic and cyclic loads. To inspect statistical variation of rupture, in each run of test, we prepare six samples under the same conditions, and load them in parallel between two rigid grippers. Under monotonic loads, using samples without initial cuts ($c = 0$) and samples with initial cuts ($c \neq 0$),we measure the rupture stretch $\lambda_c(c)$, rupture stress $S_c(c)$, and work of rupture $W_c(c)$. When the initial cut is short, the work of rupture is a material constant, $W_c(0)$, insensitive to the length of the initial cut. When the initial cut is long, we have previous measured the toughness, $G_c$, which is a material constant, insensitive to the length of the initial cut. The two material constants define the fractocohesive length, $G_c/W_c(0)$. The rupture properties $\lambda_c(c)$, $S_c(c)$, and $W_c(c)$ are sensitive to the length of initial cut when the cut length exceeds the flaw-sensitivity length $c_c$, which scales with the fractocohesive length $G_c/W_c(0)$. Under cyclic loads, using samples with and without initial cuts, we measure the endurance stretch $\lambda_e(c)$, endurance stress $S_e(c)$, and endurance work $W_e(c)$. When the initial cut is short, the endurance work is a material constant, $W_e(0)$, insensitive to the length of the initial cut. When the initial cut is long, the threshold is a material constant, $G_{th}$, insensitive to the length of the initial cut. The two material constants define the endurance fractocohesive length, $G_{th}/W_e(0)$. The endurance properties $\lambda_e(c)$, $S_e(c)$, and $W_e(c)$ are sensitive to the length of the initial cut when the initial cut exceeds the endurance flaw-sensitivity length $c_e$, which scales with $G_{th}/W_e(0)$. We compare the hydrogel and other materials in the space of material properties.

## Declaration of Competing Interest

The authors declare that they have no known competing financial interests or personal relationships that could have appeared to influence the work reported in this paper.

## Acknowledgments

TL acknowledges the support of NSFC (11922210, 11772249). JH acknowledges the support of NSFC (11702207).

## References

Abraham, F., Alshuth, T., Jerrams, S., 2013. Dependence on mean stress and stress amplitude of fatigue life of EPDM elastomers. Plast. Rubber Compos. 30, 421–425.
Ansari, M.T.A., Singh, K.K., Azam, M.S., 2018. Fatigue damage analysis of fiber-reinforced polymer composites—a review. J. Reinforced Plasti. Compos. 37, 636–654.
Bai, R., Yang, J., Morelle, X.P., Yang, C., Suo, Z., 2018. Fatigue fracture of self–recovery hydrogels. ACS Macro Lett. 7, 312–317.
Bai, R., Yang, J., Suo, Z., 2019. Fatigue of hydrogels. Eur. J. Mech. – A/Solids 74, 337–370.
Bai, R., Yang, Q., Tang, J., Morelle, X.P., Vlassak, J., Suo, Z., 2017. Fatigue fracture of tough hydrogels. Extreme Mech. Lett. 15, 91–96.
Berry, J.P., 1961. Fracture processes in polymeric materials. II. the tensile strength of polystyrene. J. Polym. Sci. 50, 313–321.
Bhowmick, A.K., N., G.A., R., P.C.T., 1983. Tear strength of elastomers under threshold conditions. Rubber Chem. Technol. 226–232.
Butcher, J.T., Mahler, G.J., Hockaday, L.A., 2011. Aortic valve disease and treatment: the need for naturally engineered solutions. Adv. Drug Deliv. Rev. 63, 242–268.
Caló, E., Khutoryanskiy, V.V., 2015. Biomedical applications of hydrogels: a review of patents and commercial products. Eur. Polym. J. 65, 252–267.
Chen, B., Yang, J., Bai, R., Suo, Z., 2019. Molecular staples for tough and stretchable adhesion in integrated soft materials. Adv. Healthc. Mater. 8, 1900810.
Chen, C., Wang, Z., Suo, Z., 2017. Flaw sensitivity of highly stretchable materials. Extreme Mech. Lett. 10, 50–57.
Culver, H.R., Clegg, J.R., Peppas, N.A., 2017. Analyte-responsive hydrogels: intelligent materials for biosensing and drug delivery. Acc. Chem. Res. 50, 170–178.
Davidge, R.W., Evans, A.G., 1970. The strength of ceramics. Mater. Sci. an Eng. 6, 281–298.
Dizon, E.S., Hicks, A.E., Chirico, V.E., 1974. The effect of carbon black parameters on the fatigue life of filled rubber compounds. Rubber Chem. Technol. 47, 231–249.
Fan, H., Gong, J.P., 2020. Fabrication of bioinspired hydrogels: challenges and opportunities. Macromolecules 53, 2769–2782.
Fleck, N.A., Kang, K.J., Ashby, M.F., 1994. Overview no. 112 the cyclic properties of engineering materials. Acta. Metall. Mater. 42, 365–381.
Gent, A.N., B., L.P., G., T.A., 1964. Cut growth and fatigue of rubbers. I. The relationship between cut growth and fatigue. J. Appl. Polym. Sci. 8, 455–466.
Gent, A.N., Tobias, R.H., 1982. Threshold tear strength of elastomers. J. Polym. Sci. Polym. Phys. 20, 2051–2058.
Gong, J.P., 2010. Why are double network hydrogels so tough? Soft Matter 6, 2583–2590.
Gong, J.P., Katsuyama, Y., Kurokawa, T., Osada, Y., 2003. Double-network hydrogels with extremely high mechanical strength. Adv. Mater. 15, 1155–1158.
Greensmith, H.W., 1956. Rupture of rubber. IV. tear properties of vulcanizates containing carbon black. J. Polym. Sci. 21, 175–187.
Greensmith, H.W., 1960. Rupture of rubber. VIII. Comparisons of tear and tensile rupture measurements. J. Appl. Polym. Sci. 3, 183–193.
Greensmith, H.W., Mullins, L., Thomas, A.G., 1960. Rupture of rubber. Trans. Soc. Rheol. 4, 179–189.

Gregg, E.C., Macey, J.H., 1973. The relationship of properties of synthetic poly(isoprene) and natural rubber in the factory. the effect of non-rubber constituents of natural rubber. Rubber Chem. Technol. 46, 47–66.
Griffith, A.A., 1921. The phenomena of rupture and flow in solids. Philoso. Trans. Royal Soc. A 221, 163–198.
Greensmith, H.W., 1964. Rupture of rubber. XI. Tensile rupture and crack growth in a noncrystallizing rubber. J. Appl. Polym. Sci. 8, 1113–1128.
Hasan, A., Ragaert, K., Swieszkowski, W., Selimovic, S., Paul, A., Camci-Unal, G., Mofrad, M.R., Khademhosseini, A., 2014. Biomechanical properties of native and tissue engineered heart valve constructs. J. Biomech. 47, 1949–1963.
Keplinger, C., Sun, J.Y., Foo, C.C., Rothemund, P., Whitesides, G.M., Suo, Z., 2013. Stretchable, transparent, ionic conductors. Science 341, 984–987.
Kim, C.C., Lee, H.H., Oh, K.H., Sun, J.Y., 2016. Highly stretchable, transparent ionic touch panel. Science 353, 682–687.
Koshut, W.J., Rummel, C., Smoot, D., Kirillova, A., Gall, K., 2020a. Flaw sensitivity and tensile fatigue of poly (vinyl alcohol) hydrogels. Macromol. Mater. Eng.
Koshut, W.J., Smoot, D., Rummel, C., Kirillova, A., Gall, K., 2020b. Tensile fatigue of poly(vinyl alcohol) hydrogels with bio-friendly toughening agents. Macromol. Mater. Eng 305.
Lake, G.J., 1972. Mechanical fatigue of rubber. Rubber Chem. Technol. 45, 309–328.
Lake, G.J., Lindley, P.B., 1966. Fatigue of rubber at low strains. J. Appl. Polym. Sci. 10, 343–351.
Lake, G.J., Thomas, A.G., 1967. The strength of highly elastic materials. Proc. R. Soc. Ser. A 11.
Lee, J.M., Sultan, M.T., Kim, S.H., Kumar, V., Yeon, Y.K., Lee, O.J., Park, C.H., 2017. Artificial auricular cartilage using silk fibroin and polyvinyl alcohol hydrogel. Int. J. Mol. Sci. 18.
Li, J., Celiz, A.D., Yang, J., Yang, Q., Wamala, I., Whyte, W., Seo, B.R., Vasilyev, N.V., Vlassak, J.J., Suo, Z., Mooney, D.J., 2017. Tough adhesives for diverse wet surfaces. Science 357, 378–381.
Li, J., Mooney, D.J., 2016. Designing hydrogels for controlled drug delivery. Nat. Rev. Mater. 1, 16071.
Lin, S.T., Liu, X.Y., Liu, J., Yuk, H., Loh, H.C., Parada, G.A., 2019. Anti-fatigue-fracture hydrogels. Sci. Adv. 5, eaau8528.
Lindley, G.J.L.a.P.B., 1964. Cut growth and fatigue of rubbers. 11. experiments on a noncrystallizing rubber. J. Appl. Polym. Sci. 8, 707–721.
Liu, M., Zeng, X., Ma, C., Yi, H., Ali, Z., Mou, X., Li, S., Deng, Y., He, N., 2017. Injectable hydrogels for cartilage and bone tissue engineering. Bone Res. 5, 17014.
Liu, Y., Liu, J., Chen, S., Lei, T., Kim, Y., Niu, S., Wang, H., Wang, X., Foudeh, A.M., Tok, J.B., Bao, Z., 2019. Soft and elastic hydrogel-based microelectronics for localized low-voltage neuromodulation. Nat. Biomed. Eng. 3, 58–68.
Masuda, F., 1994. Trends in the development of superabsorbent polymers for diapers. Superabsorbent Polym. 573, 88–98.
Masuda, M., Soma, T., Matsui, M., 1990. Cyclic fatigue behavior of Si3N4 ceramics. J. Eur. Ceramic Soc. 6, 253–258.
Nam, S., Mooney, D., 2021. Polymeric tissue adhesives. Chem. Rev.
Neogi, C., Bhowmick, A.K., Basu, S.P., 1990. Threshold tensile strength and modulus of carbon-black-filled rubber vulcanizates. J. Mater. Sci. 25, 3524–3530.
Parada, G., Yu, Y., Riley, W., Lojovich, S., Tshikudi, D., Ling, Q., Zhang, Y., Wang, J., Ling, L., Yang, Y., Nadkarni, S., Nabzdyk, C., Zhao, X., 2020. Ultrathin and robust hydrogel coatings on cardiovascular medical devices to mitigate thromboembolic and infectious complications. Adv. Healthc. Mater. 9, e2001116.
Paris, P.C., Gomez, M.P., Anderson, W.E., 1961. A rational analytic theory of fatigue. Trend. Eng. 13, 9–14.
Proctor, B.A., Whitney, I., Johnson, J.W., 1967. The strength of fused silica. Proc. R. Soc. Lond. Ser. A 297, 534–557.
Rivlin, R.S., Thomas, A.G., 1953. Rupture of rubber. I. Characteristic energy for tearing. J. Polym. Sci. 291–318.
Royo, J., 1992. Fatigue testing of rubber materials and articles. Polym. Test. 11, 325–344.
Schütz, W., 1996. A history of fatigue. Eng. Fracture Mech. 54, 263–300.
Sharma, A., Oh, M.C., Ahn, B., 2020. Recent advances in very high cycle fatigue behavior of metals and alloys—a review. Metals 10.
Tada, H., Paris, P., Irwin, G., 2000. The Analysis of Cracks Handbook. ASME Press, New York.
Tang, J., Li, J., Vlassak, J.J., Suo, Z., 2017. Fatigue fracture of hydrogels. Extreme Mech. Lett. 10, 24–31.
Thomas, A.G., 1955. Rupture of rubber. II. The strain concentration at an incision. J. Polym. Sci. 18, 177–188.
Thomas, A.G., 1958. Rupture of rubber. V. Cut growth in natural rubber vulcanizates. J. Polym. Sci. XXXI, 467–480.
Wichterle, O., Lim, D., 1960. Hydrogilic gels for biological use. Nature 185, 117.
Xiang, C., Wang, Z., Yang, C., Yao, X., Wang, Y., Suo, Z., 2020. Stretchable and fatigue-resistant materials. Mater. Today 34, 7–16.
Yang, C., Suo, Z., 2018. Hydrogel ionotronics. Nat. Rev. Mater. 3, 125–142.
Yang, C., Yin, T., Suo, Z., 2019a. Polyacrylamide hydrogels. I. network imperfection. J. Mech. Phys. Solids. 131, 43–55.
Yang, F., Zhao, J., Koshut, W.J., Watt, J., Riboh, J.C., Gall, K., Wiley, B.J., 2020. A synthetic hydrogel composite with the mechanical behavior and durability of cartilage. Adv. Funct. Mater. 30.
Yang, J., Bai, R., Chen, B., Suo, Z., 2019b. Hydrogel adhesion: a supramolecular synergy of chemistry, topology, and mechanics. Adv. Funct. Mater. 30.
Yao, X., Liu, J., Yang, C., Yang, X., Wei, J., Xia, Y., Gong, X., Suo, Z., 2019. Hydrogel Paint. Adv. Mater. 31, e1903062.
Yuk, H., Lin, S., Ma, C., Takaffoli, M., Fang, N.X., Zhao, X., 2017. Hydraulic hydrogel actuators and robots optically and sonically camouflaged in water. Nat. Commun. 8, 14230.
Yuk, H., Lu, B., Zhao, X., 2019a. Hydrogel bioelectronics. Chem. Soc. Rev. 48, 1642–1667.
Yuk, H., Varela, C.E., Nabzdyk, C.S., Mao, X., Padera, R.F., Roche, E.T., Zhao, X., 2019b. Dry double-sided tape for adhesion of wet tissues and devices. Nature 575, 169–174.
Yuk, H., Zhang, T., Parada, G.A., Liu, X., Zhao, X., 2016. Skin-inspired hydrogel-elastomer hybrids with robust interfaces and functional microstructures. Nat. Commun. 7, 12028.
Zhang, E., Bai, R., Morelle, X.P., Suo, Z., 2018a. Fatigue fracture of nearly elastic hydrogels. Soft Matter. 14, 3563–3571.
Zhang, W., Hu, J., Tang, J., Wang, Z., Wang, J., Lu, T., Suo, Z., 2018b. Fracture toughness and fatigue threshold of tough hydrogels. ACS Macro Lett. 8, 17–23.
Zhang, W., Liu, X., Wang, J., Tang, J., Hu, J., Lu, T., Suo, Z., 2018c. Fatigue of double-network hydrogels. Eng. Fract. Mech. 187, 74–93.
Zhang, W.L., Liu, X., Wang, J.K., Tang, J.D., Hu, J., Lu, T.Q., Suo, Z.G., 2018d. Fatigue of double-network hydrogels. Eng. Fracture Mech. 187, 74–93.
Zhang, Y.S., Khademhosseini, A., 2017. Advances in engineering hydrogels. Science 356, eaaf3627.
Zhou, Y., Zhang, W., Hu, J., Tang, J., Jin, C., Suo, Z., Lu, T., 2020. The stiffness-threshold conflict in polymer networks and a resolution. J. Appl. Mech. 87, 031002.